COO-1545-122

Topological Cross Sections and Correlation Functions in High Energy p p and π p Collisions*

David M. Scott, K. Tanaka, and R. Torgerson
Department of Physics
The Ohio State University
Columbus, Ohio 43210

ABSTRACT

We study a two component model in which the dominant non-diffractive component possesses Koba, Nielsen and Olesen scaling and the other component is diffractive. This model is fit to the available p p and $\pi^{\pm}$p topological cross sections above 10 GeV/c, and is used to make predictions at higher energies. For purposes of comparison, a one component scaling model is also considered.

*Research supported in part by the U.S. Atomic Energy Commission under Contract AT(11-1)-1545

DISCLAIMER

I. INTRODUCTION

There has been a great deal of interest in the topological cross sections for n charged particle production σ_n and the n particle correlation functions f_n at very high energies because they may lead to an understanding of the production mechanism. Many models have been discussed which can explain some features of σ_n and f_n.[1]

It is a remarkable empirical fact[2] that at Serpukhov and NAL energies (50 - 303 GeV/c) the function $\psi = \langle n \rangle \sigma_n/\sigma_{in}$, where $\langle n \rangle$ is the average charged multiplicity and σ_{in} is the inelastic cross section, may depend only on $x = n/\langle n \rangle$. Thus, it is independent of energy and exhibits a new type of scaling. This scaling has been shown by Koba, Nielsen and Olesen to follow from the Feynman scaling property of inclusive cross sections and indicates the possibility of long range correlations.[3]

It appears that a single scaling component is an oversimplified picture so that some non-scaling correction ought to be present, especially when lower energy data are considered. It is, therefore, of interest to study models in which a non-scaling component is used to correct the predictions of scaling. The general idea of two component models was first discussed by Wilson, and later by others.[4]

The basic assumption of our two component model is that σ_n consists of two parts: the dominant part σ_{na} arises through a non-diffractive or pionization process. The other part σ_{nb} is due to an energy independent diffractive process and is non-vanishing for low multiplicities. Possible interference terms are neglected.[4]

In the present article, we take a phenomenological approach and attempt to fit the data with such a two component model. The plan of the article is

to discuss the formalism in Sec.II, the p p collisions in Sec.III and π p collisions in Sec.IV. Finally, some remarks and predictions are made in Sec.V.

II. FORMALISM

In the present model, the dominant component a satisfies KNO scaling, and the remaining component b is chosen as a Poisson distribution in the negatively charged particles;[5]

$$n_a \sigma_{an}/\sigma_a = \psi_a = N x^m e^{-\alpha x^2} \qquad (n \text{ even}), \tag{1}$$

$$n_b \sigma_{bn}/\sigma_b = \psi_b = n_b e^{-\frac{1}{2}(n_b-Q)} \left[\tfrac{1}{2}(n_b-Q)\right]^{\frac{1}{2}(n-Q)} / \left[\tfrac{1}{2}(n-Q)\right]!, \qquad (n \text{ even}) \tag{2}$$

where the subscript specifies the production mechanism, and

$$x = n/\langle n\rangle, \qquad n_a = \langle n\rangle_a, \qquad n_b = \langle n\rangle_b,$$

$$\sigma_a + \sigma_b = \sigma_{in}, \quad \sigma_a/\sigma_{in} = a, \quad \sigma_b/\sigma_{in} = b, \tag{3}$$

and Q is the total charge of the reaction, i.e.,

$$Q = 2 \text{ for } p\,p,\ \pi^+ p \quad \text{and} \quad Q = 0 \text{ for } \pi^- p.$$

Then it follows from (1)-(3)

$$\langle n^q \rangle = \sum n^q \sigma_n / \sigma_{in} = a \sum n^q \sigma_{an} / \sigma_a + b \sum n^q \sigma_{bn} / \sigma_b$$
$$= a\, n_a^q\, C_q + b\, e^{-l_b} \left(Q + 2 \frac{\partial}{\partial (\ln l_b)} \right)^q e^{l_b} , \tag{4}$$

where

$$C_q = \left[\Gamma\left(\frac{m+1}{2}\right) \right]^{q-1} \Gamma\left(\frac{m+q+1}{2}\right) \Big/ \left[\Gamma\left(1 + \frac{m}{2}\right) \right]^q , \tag{5}$$

and

$$l_b = (n_b - Q)/2 = \langle n_- \rangle , \tag{6}$$

where the sum is over even multiplicities, and for the first component a, the sum is converted to an integral.[6] The requirements

$$\sum \sigma_n / \sigma_{in} = 1 , \tag{7}$$

and

$$\langle n \rangle = a\, n_a + b\, n_b \tag{8}$$

are satisfied. In the present work, a and n_b are taken to be energy independent so that n_a varies linearly with $\langle n \rangle$. This is in conformity to the notion that diffraction is energy independent.

To calculate the n particle correlation functions, we make use of the generating function

$$F(h) = \sum (1+h)^n \sigma_n / \sigma_{in}$$
$$= \sum_{n = Q,\, Q+2, \cdots} (1+h)^n (\sigma_{an} + \sigma_{bn}) / \sigma_{in} . \tag{9}$$

The quantity in F(h) is expanded in powers of h

$$\ln F(h) = \sum_{\ell=1}^{\infty} h^{\ell} f_{\ell} / \ell! \,. \tag{10}$$

One then obtains[7]

$$f_{\ell} = \ell! \sum_{p=1}^{\ell} (-1)^{p+1} \sum_{a_1, a_2, \cdots} \frac{(p-1)!\, A_1^{a_1} A_2^{a_2} \cdots A_{\ell}^{a_{\ell}}}{(1!)^{a_1} a_1!\, (2!)^{a_2} a_2! \cdots (\ell!)^{a_{\ell}} a_{\ell}!} \,, \tag{11}$$

$$A_{\ell} = \sum \frac{n!}{(n-\ell)!} \left(a \frac{\sigma_{an}}{\sigma_a} + b \frac{\sigma_{bn}}{\sigma_b} \right) = \langle n(n-1) \cdots (n-\ell+1) \rangle \,, \tag{12}$$

with $a_1 + 2a_2 + \cdots + \ell a_{\ell} = \ell$

and $a_1 + a_2 + \cdots + a_{\ell} = p$.

The generalization of ψ_a and ψ_b that is denoted by ψ is given with the aid of Eqs. (1), (2) and (8) as

$$\langle n \rangle \sigma_n / \sigma_{in} = \psi = (a n_a + b n_b)(\sigma_{an} + \sigma_{bn}) / \sigma_{in}$$

$$= a^2 \psi_a(n/n_a) + b^2 \psi_b(n, n_b) + ab\{n_a \psi_b / n_b + n_b \psi_a / n_a\} \,. \tag{13}$$

The diffractive dissociation part b which has a constant cross section is associated with low multiplicities so that n_b is treated as a constant and the logarithmic growth of the average multiplicity arises from the part a.

We now consider the two particle correlation functions. In the two component model, one obtains the two charged particle correlation functions from (11) and (12):

$$f_2 = A_2 - A_1^2$$
$$= a\langle n(n-1)\rangle_a + b\langle n(n-1)\rangle_b - (a n_a + b n_b)^2$$
$$= a f_{a2} + b f_{b2} + ab(n_a - n_b)^2, \tag{14}$$

where

$$f_{i2} = \langle n(n-1)\rangle_i - n_i^2 = D_i^2 - n_i, \quad (i = a, b). \tag{15}$$

The two particle correlation function for negatively charged particles is defined as

$$f_2^- = \langle n_-^2\rangle - \langle n_-\rangle - \langle n_-\rangle^2. \tag{16}$$

The term $\langle n_-^2\rangle$ can be expressed in terms of products of $\langle n_-\rangle$ with the aid of Eqs.(5) and (8) so that

$$f_2^- = \left(\frac{C_2}{a} - 1\right)\langle n_-\rangle^2 + \left\{\frac{C_2}{a}(Q - b n_b) - Q - 1\right\}\langle n_-\rangle$$
$$+ \left\{\frac{C_2}{4a}(Q - b n_b)^2 + \frac{b}{4}(n_b^2 + 2n_b - 2Q) - \frac{Q^2}{4}\right\}$$
$$= \frac{1}{4}\{f_2 + 2Q - \langle n\rangle\}. \tag{17}$$

Another quantity of interest is the dispersion $D = (\langle n^2 \rangle - \langle n \rangle^2)^{\frac{1}{2}}$, that was found by Wroblewski[8] to satisfy a linear law $D = A\langle n \rangle - B$, with A, B constant in inelastic hadron collisions at high energy.[9] In the present two-component model, one obtains from (5)

$$D = \left[(A\langle n \rangle - B)^2 + C \right]^{\frac{1}{2}}, \tag{18}$$

where

$$A = \left(\frac{C_2}{a} - 1 \right)^{\frac{1}{2}}, \tag{19}$$

$$B = b C_2 n_b \Big/ \left[a \left(\frac{C_2}{a} - 1 \right)^{\frac{1}{2}} \right], \tag{20}$$

$$C = b \left\{ \frac{a(C_2 - 1) n_b^2}{C_2 - a} + 2n_b - 2Q \right\}. \tag{21}$$

We note that if C of (21) is small compared to $(A\langle n \rangle - B)^2$, it follows from Eq.(18) that

$$D = A\langle n \rangle - B. \tag{22}$$

The validity of Eq.(22) in the context of our model is discussed in Sec.V.

III. p p COLLISIONS

The p p topological cross sections[10] at 50, 69, 102, 205, 303 GeV/c have been fit very well by Slattery[11] and Weisberg[12] with one component that has KNO scaling. We are interested in the question of whether or not the diffractive component b is needed when the lower energy p p data[13] from 10 to 50 GeV/c are combined with the above data.

For this purpose, we fit the ψ given by Eq.(13) to the data. We take as free parameters m, a, n_b, and $\langle n \rangle$ in which m, a, and n_b are energy independent constants, whereas $\langle n \rangle$ is chosen to be the experimental average multiplicity of a given energy.

The momenta of the data used are listed in Table I as are the results. We can obtain a one-component effective scaling model by setting a = 1 which is also listed in Table I. The χ^2 fit for both the one- and two-component models deteriorates with the addition of the 10 and 19 GeV/c data, but the second component does improve the fit. When we add 24.14 GeV/c data, however, the χ^2 nearly doubles although we added only 7 data points (see lines 5 and 6 of Table I). Since the parameters actually change by only a few percent, we retain a measure of confidence in our parameters. Our best two-component parameters are m = 1.7, a = 0.86 and n_b = 3.7 (line 3 of Table I).

In Fig. 1, we have indicated the quality of our fit to the multiplicity data by comparing our two-component ψ with the p p data at 10 GeV/c and at 303 GeV/c. We note a slow energy dependence of our two-component Ψ over the range of data that is fitted. Therefore, we do not present the one-component ψ for p p and π p collisions.

One can also compare the one- and two-component models by examining the two particle correlation functions f_2.

The correlation function f_2^- for negative charged particles is given by Eq.(17). In Fig.2, the two-component model is compared with the one-component effective scaling model (a = 1) and with the f_2^- data. In addition, we have illustrated the effect of changing the normalization from the summation method (in which C_2 varies slightly with $\langle n \rangle$) to the integration method[6,14] [in which C_2 is fixed by Eq.(5)]. The result of the two methods differs slightly at low $\langle n_- \rangle$ and becomes asymptotically identical at higher $\langle n_- \rangle$.

In Fig.3, the dispersion D is obtained by using the summation method and Eq.(13), and is compared with the data as well as the one-component effective scaling model. One observes from Figs. 2 and 3 that the two-component model is preferred over the one-component effective scaling model.

IV. $\pi^{\pm}$ p COLLISIONS

The previous analysis of Sec. III for p p collisions is extended to $\pi^{\pm}$p collisions. In contrast to the p p case, corresponding data at NAL energies are not presently available so that one must make predictions at high energies based on data at relatively low momenta 10 GeV/c to 60 GeV/c.[15,16,17]

The ψ given by Eq.(13) is fitted in a similar manner to the p p case and the results are given for π^+p and π^-p in Tables II and III, respectively. In the π^+p case, we find m = 2.9, a = 0.77 and n_b = 4.2. (See line 3 of Table II.) We note the improvement of the fit by the second component. In the π^-p case, the quality of the fit is very poor when we include all the data. Nevertheless, we think that the parameters derived from this data set:

$m = 1.9$, $a = 0.95$ and $n_b = 3.4$ (see line 7 of Table III) is our best estimate since we cannot resolve inconsistencies in the data. (See Table III and Figs.7 and 9.)

The ψ for π^+p and π^-p are given in Figs. 4 and 5, respectively, for the highest momentum 60 GeV/c for $\pi^\pm p$, and the lowest momentum 16 GeV/c for π^+p and 10 GeV/c for π^-p. In Figs.6 and 7, the two particle correlation functions f_2^- are calculated by the summation method[14] and are compared to the data. In Figs.8 and 9, the dispersions D are given and compared to the data. We find that for the π^+p case the two-component model is definitely preferred, whereas for the π^-p case the two-component model is slightly better than the one-component effective scaling model.

In contrast to the situation above in which all the data are considered, we finally observe that for the highest available data (40 GeV/c and above), there is no preference between the one and two component models in p p and π^+p collisions, and the two component model is preferred for the π^-p collisions (see Tables I-III).

V. REMARKS AND PREDICTIONS

It has become increasingly clear that a simplified one component model of a diffractive Pomeron exchange component or a non-diffractive (multiperipheral or pionization) component does not provide a reasonable fit to high energy data on p p and $\pi^\pm p$ collisions such as the topological cross sections, and two particle correlations.

We consider a two component model in which the dominant first non-diffractive component effectively satisfies KNO scaling. The second diffractive component is energy independent and satisfies a Poisson distribution in the negatively charged particles. We hope that this model

is applicable to p p and $\pi^{\pm}$p collisions above 10 GeV/c. Recently, the high energy p p collision data have been fitted in several papers in the framework of a two component model.[18] The present paper differs from all of these in the choice of one component that satisfies KNO scaling.

Let us now discuss the dispersion D obtained in Sec. II, and compare our results with the data and Wroblewski's result[8] on the linearity of D versus $\langle n \rangle$. We note from Eqs. (18) and (21) that

$$D = (C_2 - 1)^{\frac{1}{2}} \langle n \rangle , \tag{23}$$

in the scaling model (b = 0). This raises the following questions. Can D be represented by a straight line, and, if so, does the curve extrapolate to D = 0 at $\langle n \rangle$ = 0? We find from Fig. 3 that the dispersions from both models have a slight curvature. The departure of the effective scaling model from Eq. (23) is due to the fact that we normalize the a component with the summation method.[6] If, in addition, we calculate the parameters A, B. and C of Eqs. (18) and (22) for p p collisions, we find A = 0.63, B = 1.15 and C = 1.4 in our two component model in contrast to Wroblewski's[8] A = B = 0.585.

We find A = 0.69, B = 2.07 and C = 2.2 for π^{+}p, and A = 0.50, B = 0.40, C = 0.70 for π^{-}p. These values should be compared to A = 0.44, B = 0.09 for π^{+}p and A = 0.44, B = 0.22 for π^{-}p given in Ref. 8. In the π^{+}p case, the curvature is considerable (see Fig. 8) in disagreement with Ref. 8, whereas in the π^{-}p case, we are in agreement (see Fig. 9). In general, the D of the two component model approaches the linear function Eq. (23) for sufficiently large average multiplicities $\langle n \rangle$.

We now consider the quantity $\psi = \langle n \rangle \sigma_n / \sigma_{in}$. We observe in Fig.1 that the ψ for p p given by our two component model, is nearly the same at 10 and 303 GeV/c. It appears on geometrical grounds that a plot of ψ versus $n/\langle n \rangle$ should be roughly energy independent. The same phenomena occur for $\pi^+ p$ and $\pi^- p$ as indicated in Figs.4 and 5. We expect that the curves of ψ given in Figs.1,4 and 5 should resemble similar plots of ψ at higher energies.

In order to predict ψ at higher energies, a reasonably accurate value of $\langle n \rangle$ is all that is required, since all the other parameters have been estimated. In the case of p p collisions, we take[19] $\langle n \rangle = 9.5$ for $p_{lab} = 500$ GeV/c, $\langle n \rangle = 11.7$ for $p_{lab} = 1500$ GeV/c, and $\langle n \rangle = 16.3$ for $p_{lab} = 10{,}000$ GeV/c. It is to be noticed in Fig.10 that the second component is becoming visible at $p_{lab} = 1500$ GeV/c giving rise to the low multiplicity bump-dip-bump structure. This is a well known property of two component models.[20] This feature is more prominent if σ_n/σ_{in} is plotted versus n. As energy increases, the a component is spreading out and reducing in absolute value whereas the b component is fixed (see Fig.11).

In a similar manner, we present our prediction[21] of ψ and σ_n/σ_{in} for $\pi^+ p$ and $\pi^- p$ in Figs.12-14. Note that a graph of ψ for $\pi^- p$ is not given, since the 60 GeV/c curve of Fig.5 adequately represents the result. This is due to the fact that the $\pi^- p$ parameters approximate those of pure scaling.

Clearly, it is not possible to choose between the present one component model and our two component model. Higher energy π p multiplicity data from NAL and p p data from the ISR would be helpful in making a choice.

It is extremely interesting from our point of view to find out what the present and previous [2,12] phenomenological models that have KNO scaling models reveal about the underlying production mechanisms. Various attempts

in this direction have been made recently,[3,22] which may lead to a better understanding of high energy collisions.

ACKNOWLEDGEMENTS

One of us (K.T.) is grateful to Z. Koba for stimulating discussions and to A. Bohr and Z. Koba for their hospitality at the Niels Bohr Institute. Another (R.T.) wishes to thank Lai-Him Chan for enlightening discussions about KNO phenomenology. The authors wish to thank The Ohio State University Instruction and Research Computer Center and the High Energy Experimental Group for the use of their computers.

REFERENCES

1. See, for example, M. Jacob, in Proceedings of the Sixteenth International Conference on High Energy Physics, National Accelerator Laboratory, Batavia, Illinois, 1972 (to be published); M. Le Bellac, in Proceedings of the Sixteenth International Conference on High Energy Physics, National Accelerator Laboratory, Batavia, Illinois, 1972 (to be published).
2. P. Olesen, Phys. Letters 41B, 602 (1972); P. Slattery, Phys. Rev. Letters 29, 1624 (1972), University of Rochester Report No. UR-409, 1972 (to be published).
3. Z. Koba, H. B. Nielsen and P. Olesen, Nucl. Phys. B40, 317 (1972).
4. K. G. Wilson, Cornell University Report No. CLNS-131, 1970; K. Fiałkowski, Phys. Letters 41B, 379 (1972); A. Bialas, K. Fiałkowski and K. Zalewski, Nucl. Phys. B48, 237 (1972).
5. The charged particle multiplicity distribution σ_n/σ_{in} cannot be a Poisson distribution because it vanishes for odd n. We feel that the precise form of the b component is relatively unimportant because it is the small component.
6. The equations $\Sigma\sigma_{an} = \sigma_a$, $\Sigma n\, \sigma_{an} = n_a$ lead to $N = 4\Gamma\left[\left(1 + \frac{m}{2}\right)\right]^{m+1} / \left[\Gamma\left(\frac{m+1}{2}\right)\right]^{m+2}$ and $\alpha = \left[\Gamma\left(1 + \frac{m}{2}\right)/\Gamma\left(\frac{m+1}{2}\right)\right]^2$ in Eq. (1), when the sums are converted into integrals. We refer to this as the integration method. Actually, for our work, numerical summation is always performed. This is referred to as summation method. The comparison of the methods is discussed in Sec. III. (See also Fig. 2.) In case the summation method is used, N and α of Eq. (1) have a slight energy dependence which effectively disappears beyond 60 GeV/c. We refer to this situation in

Eq.(1) as effective KNO scaling.

7. An equivalent form for f_ℓ may be found in A. H. Mueller, Phys. Rev. D 4, 150 (1971).

8. A. Wroblewski, Warsaw University Report No. IFD 72/2, 1972.

9. L. Van Hove, Phys. Letters 43B, 65 (1973).

10. p_{lab} = 50,69 GeV/c, V. V. Ammosov et al., Phys. Letters 42B, 519 (1972); p_{lab} = 102 GeV/c, J. W. Chapman et al., Phys. Rev. Letters 29, 1686 (1972); p_{lab} = 205 GeV/c, G. Charlton et al., Phys. Rev. Letters 29, 515 (1972); p_{lab} = 303 GeV/c, F. T. Dao et al., Phys. Rev. Letters 29, 1672 (1972). We have actually used the table of values and errors given by Slattery in Ref. 2 for our χ^2 program, which means that our χ^2 values for the one component fit to the 50 - 303 GeV/c data may be compared directly with those of Refs. 2 and 12. Since the errors given by Slattery are smaller on the average than those given in the experimental papers, we have reduced by a factor of 0.97 the errors on the 10 GeV/c and 24.12 GeV/c data. This is not done in the π^+p and π^-p cases.

11. P. Slattery (Ref.2).

12. H. Weisberg, University of Pennsylvania Report No. UPR-0015T, 1973.

13. p_{lab} = 10 GeV/c, S. P. Almeida et al., Phys. Rev. 174, 1638 (1968); p_{lab} = 19 GeV/c, H. Bøggild et al., Nucl. Phys. B27, 285 (1971); p_{lab} = 24.12 GeV/c, D. B. Smith et al., Phys. Rev. Letters 23, 1064 (1969). At 24.12 GeV/c, σ_2 is taken from J. Hanson et al. CERN/HERA Report No. 70-2, 1970.

14. For the summation method, we use

$$f_2^- = \sum_{n_-} \left\{ \left(a/n_a\right)\psi_a\left[(2n_- + Q)/n_a\right] + \left(b/n_b\right)\psi_b(2n_- + Q, n_b) \right\} \left[n_-(n_- - 1) - \langle n_- \rangle^2 \right]$$

where ψ_a and ψ_b are given in Eqs.(1) and (2). This is equivalent to using Eq.(17) with $C_2 = \sum_n n^2 \psi_a / n_a^3$.

15. p_{lab} = 16 GeV/c, J. Ballam et al., Phys. Rev. 3, 2606 (1971); ABBCCW Collaboration, to be published. The weighed average of these two experiments is used. The $\sigma_{2\ in}$ is calculated from σ_2 and $\sigma_{2\ el}$. The value of $\sigma_{2\ el}$ comes from the fitted curve on p.161 of E. Bracci et al., CERN/HERA Report No. 72-1, 1972.

p_{lab} = 18.5 GeV/c, J. T. Powers, Ph.D. Thesis, University of Notre Dame; N. N. Biswas (private communication).

p_{lab} = 40 GeV/c, O. Balea et al., Nucl. Phys. B52, 414 (1972) (π^-n).

p_{lab} = 45 and 60 GeV/c, E. V. Anzon et al., Phys. Letters 31B, 237 (1970) (π^-n).

16. We have read the multiplicity distribution for π^-p and π^-n from the histograms presented in E. V. Anzon et al.[15], using the square root of the number of events as the measure of the error in the number of events. The average value of $\langle n \rangle$, i.e., 5.98 ± 25, that we derive this way for 45 GeV/c π^-p is lower than their quoted value 6.10 ± 28. This is the largest discrepancy in all the data that we have used. Normally, there is no discrepancy. Our policy has been to use the $\langle n \rangle$ computed from the multiplicity distribution data in our χ^2 minimization program to keep the arithmetic internally consistent. In our plots of D or f_2^-, however, the results quoted in experimental papers are used, in preference to the ones we calculate from multiplicity data wherever such results

are available. We derive the π^+p multiplicity distribution from the π^-n distribution by isospin invariance. If the probability distribution for π^-n is $P_{\pi^-n}(n)$, then $P_{\pi^+p}(n) = P_{\pi^-n}(n-1)$. This relation was checked for low number of final state particles; we have not yet worked through a formal proof.

17. p_{lab} = 10 GeV/c, P. Fleury et al., in Proceedings of the 1962 International Conference on High Energy Physics at CERN, p.597;
M. Bardadin, Institute of Nuclear Research (Warsaw) Report No. INR 511/6-64, 1964.
p_{lab} = 13 GeV/c, G. W. Brandenburg et al., Nucl. Phys. B16, 287 (1970).
p_{lab} = 16 GeV/c, S. J. Goldsack et al., Nuovo Cimento 23, 941 (1970);
R. Honecker et al., Nucl. Phys. B13, 571 (1969);
J. Balam et al., Phys. Rev. 3, 2606 (1971). The weighted average of these three experiments is used.
p_{lab} = 18.5 GeV/c, J. T. Powers, Ph.D. Thesis, University of Notre Dame;
N. N. Biswas (private communication).
p_{lab} = 20 GeV/c, G. W. Brandenburg et al., Nucl. Phys. B16, 287 (1970).
p_{lab} = 25 GeV/c, J. W. Elbert et al., Nucl. Phys. B19, 85 (1970).
p_{lab} = 40 GeV/c, O. Balea et al., Nucl. Phys. B52, 414 (1972).
p_{lab} = 45 and 60 GeV/c, E. V. Anzon et al., Phys. Letters 31B, 237 (1970).

18. W. R. Frazer, R. D. Peccei, S. S. Pinsky and C.-I. Tan, University of California, San Diego Report No. UCSD-10P10-113, 1972;
C. Quigg and J. D. Jackson, National Accelerator Laboratory Report No. NAL-THY-93, 1972;
H. Harari and E. Rabinovici, Phys. Letters 43B, 49 (1973);
K. Fiałkowski and H. J. Miettinen, Phys. Letters 43B, 61 (1973).

19. In case of p p collisions, we use values of $\langle n \rangle$ to be found in M. Jacob, Ref.1. In case more than one value is given, we take the weighted averages.

20. K. G. Wilson (Ref.4).

21. Our predictions are based on a reasonable estimate of $\langle n \rangle$ since it is outside the scope of the present approach to calculate $\langle n \rangle$. For the $\pi^{\pm} p$ case, data on $\langle n \rangle$ is plotted versus log p_{lab}. For $\pi^{+} p$, we extrapolate and obtain $\langle n \rangle = 8$ and 9 for 100 and 200 GeV/c, respectively. For $\pi^{-} p$, we used the value $\langle n \rangle = 8.0 \pm 0.17$ (200 GeV/c) given by F. R. Huson et al., International Conference on New Results from Experiments on High Energy Particle Collisions, Vanderbilt University, Nashville, Tennessee, 1973, and interpolate to get the value $\langle n \rangle = 7.4$ at 100 GeV/c.

22. For example, Z. Koba, H. B. Nielsen and P. Olesen, Nucl. Phys. B40, 317 (1972); P. Suranyi, University of Cincinnati preprints (unpublished); S. Barshay, Phys. Letters 42B, 457 (1972); H. B. Nielsen and P. Olesen Phys. Letters 43B, 37 (1973); G. Aubrecht, K. Tanaka and R. Torgerson (in preparation).

Table I.

Model Parameters for $\psi = \langle n \rangle \sigma_n/\sigma_{in}$ in p p Collisions

Momenta Used (GeV/c)								Fitted Parameters			χ^2	Number of Data Points	Model
10	19	24	50	69	102	205	303	m	a	n_b			
			x	x	x	x	x	1.14	0.99	4.4	46	50	2-component
			x	x	x	x	x	1.12	1		46	50	1-component
x	x		x	x	x	x	x	1.7	0.86	3.7	113	61	2-component
x	x		x	x	x	x	x	1.4	1		171	61	1-component
x	x	x	x	x	x	x	x	1.9	0.83	3.9	216	68	2-component
x	x	x	x	x	x	x	x	1.6	1		321	68	1-component

Table II

Model Parameters for $\psi = \langle n \rangle \sigma_n/\sigma_{in}$ in $\pi^+ p$ Collisions

Momenta Used (GeV/c)					Fitted Parameters			χ^2	Number of Data Points	Model
16	18.5	40	45	60	m	a	n_b			
		x	x	x	2.3	0.69	5.0	25	25	2-component
		x	x	x	1.6	1		30	25	1-component
x	x	x	x	x	2.9	0.77	4.2	77	37	2-component
x	x	x	x	x	2.2	1		142	37	1-component

Table III

Model Parameters for $\psi = \langle n \rangle \sigma_n/\sigma_{in}$ in $\pi^- p$ Collisions

Momenta Used (GeV/c)									Fitted Parameters			χ^2	Number of Data Points	Model
10	13	16	18.5	20	25	40	45	60	m	a	n_b			
						x	x	x	1.6	0.78	6.8	36	29	2-component
						x	x	x	1.4	1		91	29	1-component
x		x				x	x	x	1.7	0.95	2.7	98	42	2-component
x		x				x	x	x	1.8	1		206	42	1-component
	x		x	x	x	x	x	x	2.0	0.95	3.4	172	61	2-component
	x		x	x	x	x	x	x	1.8	1		330	61	1-component
x	x	x	x	x	x	x	x	x	1.9	0.95	3.2	201	74	2-component
x	x	x	x	x	x	x	x	x	1.7	1		392	74	1-component

FIGURE CAPTIONS

Fig. 1. Plot of $\psi = \langle n \rangle \sigma_n/\sigma_{in}$ versus $(n/\langle n \rangle)$ for p p → n charged particles at 10 and 303 GeV/c. The curves are the two component fit of Eq.(13). The values of the parameters are m = 1.7, a = 0.86 and $n_b = 3.7$.

Fig. 2. Plot of two particle correlation function f_2^- versus $\langle n_- \rangle$ for p p → negative particles at momenta 10, 19, 24, 50, 69, 102, 205 and 303 GeV/c. The curves represent the one component fit m = 1.4, a = 1 and the two component fit m = 1.7, a = 0.86, $n_b = 3.7$, using both the sum and integral methods.

Fig. 3. Plot of dispersion D versus $\langle n \rangle$ for p p → charged particles at momenta 10, 19, 24, 50, 69, 102, 205 and 303 GeV/c. The curves represent the one and two component fits.

Fig. 4. Plot of $\psi = \langle n \rangle \sigma_n/\sigma_{in}$ versus $(n/\langle n \rangle)$ for $\pi^+ p \rightarrow$ n charged particles at 16 and 60 GeV/c. The curves are the two component fit of Eq.(13). The parameters are m = 2.9, a = 0.77 and $n_b = 4.2$.

Fig. 5. Plot of $\psi = \langle n \rangle \sigma_n/\sigma_{in}$ versus $(n/\langle n \rangle)$ for $\pi^- p \rightarrow$ n charged particles at 10 and 60 GeV/c. The curves are the two component fit of Eq.(13). The parameters are m = 1.9, a = 0.95 and $n_b = 3.4$.

Fig. 6. Plot of two particle correlation function f_2^- versus $\langle n_- \rangle$ for $\pi^+ p \rightarrow$ negative particles at momenta 16, 18.5, 40, 45 and 60 GeV/c. The curves represent the one and two component fits.

Fig. 7. Plot of two particle correlation function f_2^- versus $\langle n_- \rangle$ for $\pi^- p \rightarrow$ negative particles at momenta 10, 13, 16, 18.5, 20, 25, 40, 45 and 60 GeV/c. The curves represent the one and two component fits.

Fig. 8. Plot of dispersion D versus $\langle n \rangle$ for $\pi^+ p \rightarrow$ n charged particles at momenta 16, 18.5, 40, 45 and 60 GeV/c. The curves represent the one and two component fits.

Fig. 9. Plot of dispersion D versus $\langle n \rangle$ for $\pi^- p \rightarrow$ n charged particles at momenta 10, 13, 16, 18.5, 20, 25, 40, 45 and 60 GeV/c. The curves represent the one and two component fits.

Fig.10. The two component result for $\psi = \langle n \rangle \sigma_n/\sigma_{in}$ versus $n/\langle n \rangle$ obtained from Eq.(13) for p p $\rightarrow$ n charged particles at 500, 1500 and 10,000 GeV/c.

Fig.11. The two component result for σ_n/σ_{in} versus n for p p $\rightarrow$ n charged particles obtained from $\psi/\langle n \rangle$ [Eq.(13)] at 500, 1000, 1500 and 10,000 GeV/c. The energy independent b component is also presented.

Fig. 12. The two component results for $\psi = \langle n \rangle \sigma_n/\sigma_{in}$ versus $n/\langle n \rangle$ obtained from Eq. (13) for $\pi^+ p \rightarrow n$ charged particles at 100 and 200 GeV/c.

Fig. 13. The two component results for σ_n/σ_{in} versus n for $\pi^+ p \rightarrow n$ charged particles obtained from $\psi/\langle n \rangle$ [Eq. (13)] at 100 and 200 GeV/c.

Fig. 14. The two component results for σ_n/σ_{in} versus n for $\pi^- p \rightarrow n$ charged particles obtained from $\psi/\langle n \rangle$ [Eq. (13)] at 100 and 200 GeV/c.

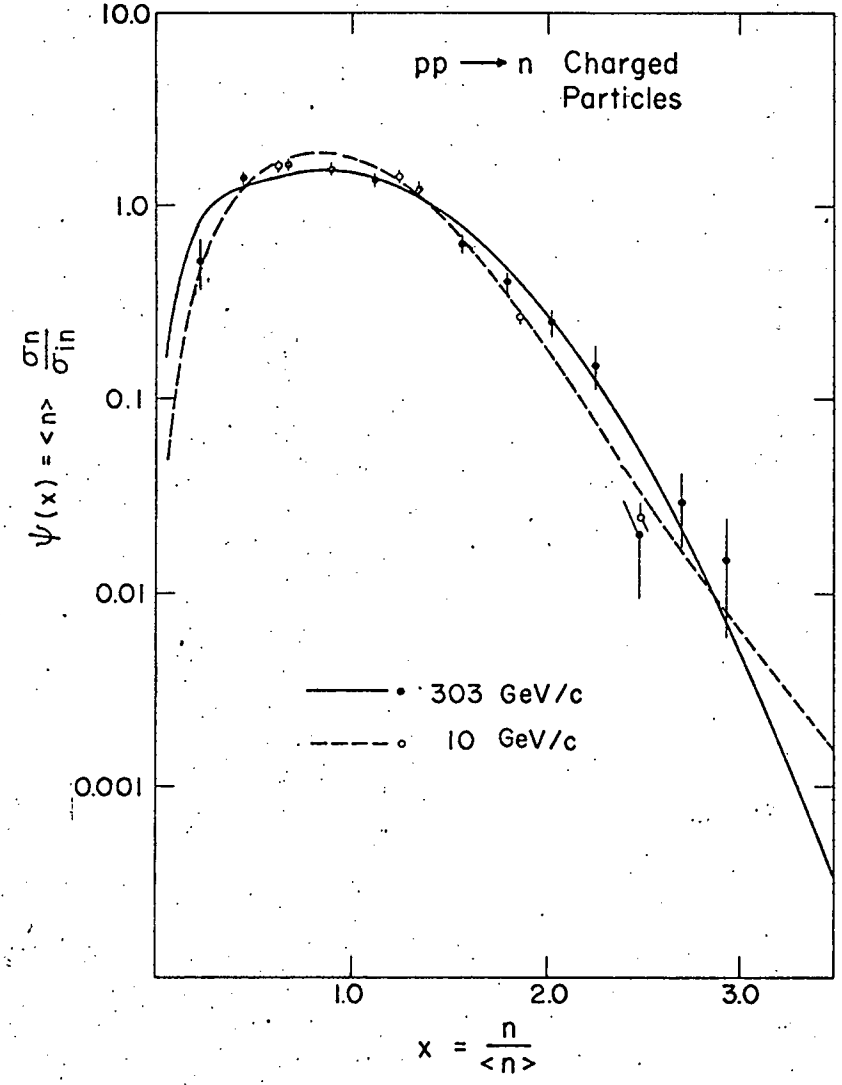
pp → n Charged Particles
10.0
1.0
0.1
0.01
0.001
$\psi(x) = \langle n \rangle \frac{\sigma_n}{\sigma_{in}}$
303 GeV/c
10 GeV/c
1.0
2.0
3.0
$x = \frac{n}{\langle n \rangle}$

Fig. 1

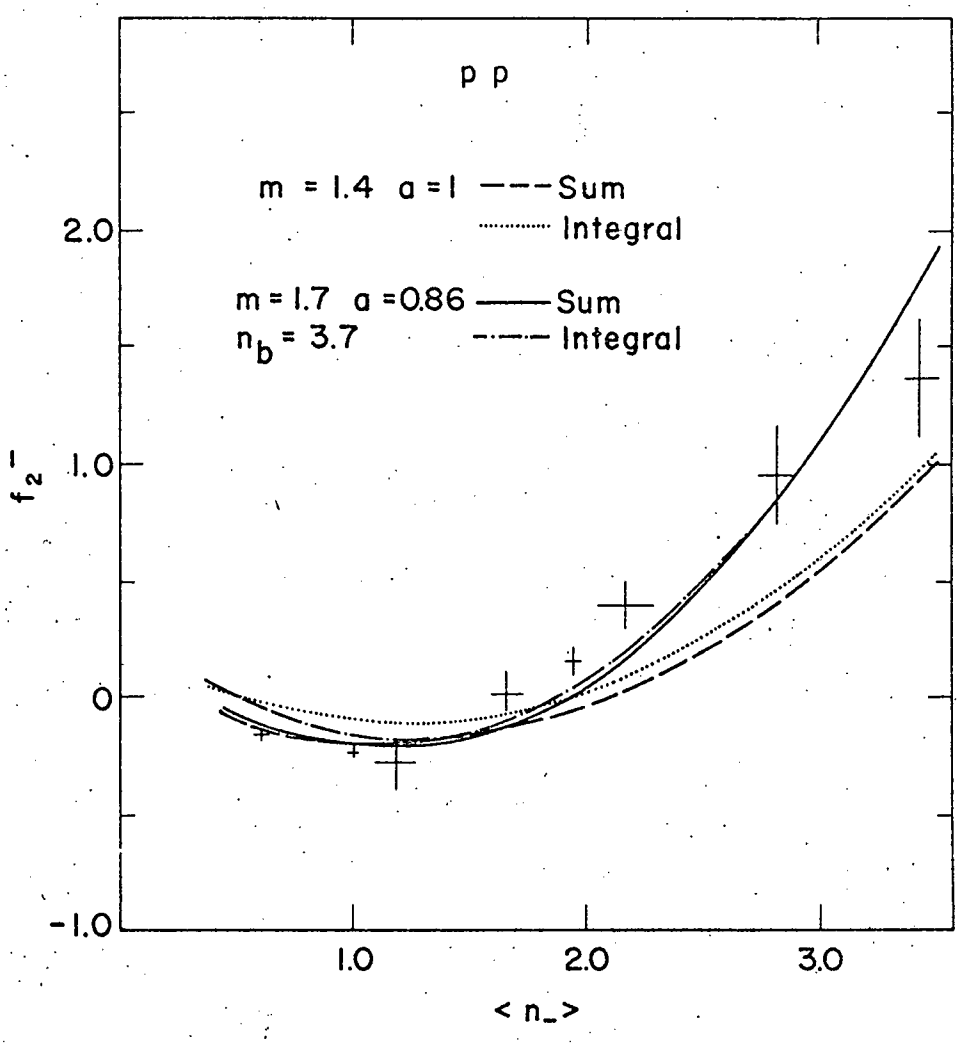
p p
m = 1.4 a = 1 Sum
Integral
m = 1.7 a = 0.86 Sum
n_b = 3.7 Integral
2.0
1.0
0
-1.0
f_2^-
1.0
2.0
3.0
$\langle n_- \rangle$

Fig. 2

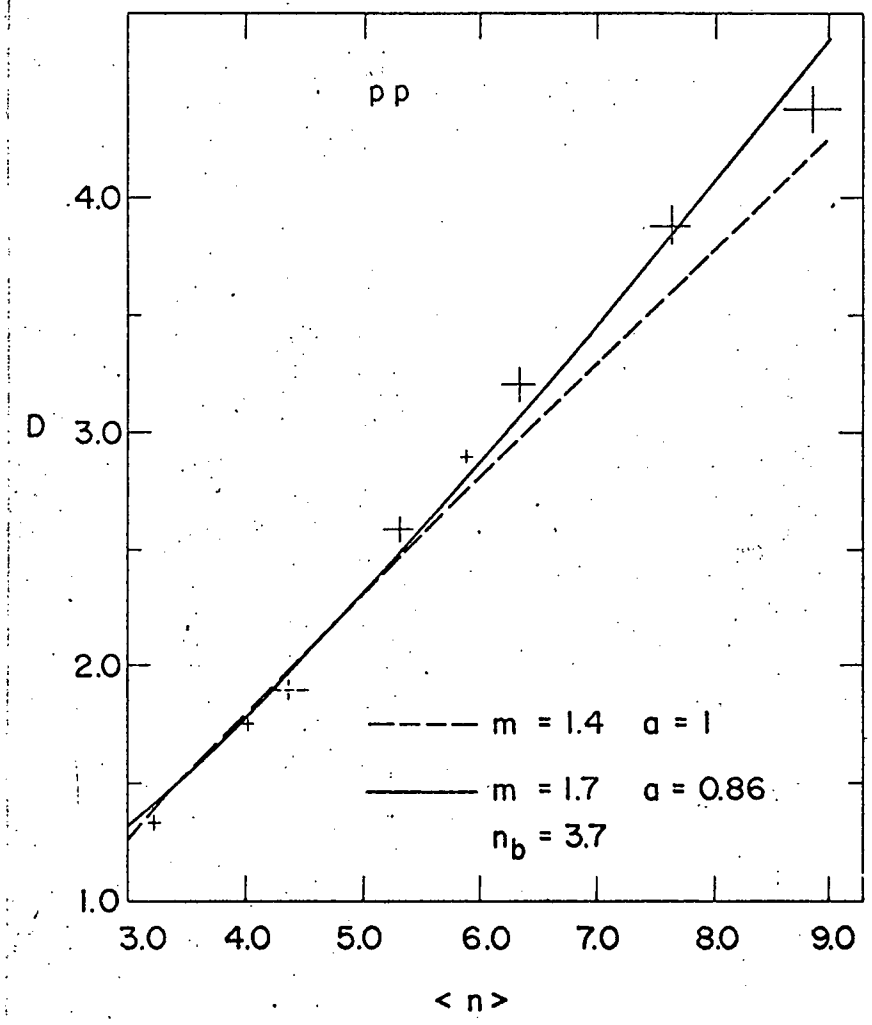
p p
D
4.0
3.0
2.0
1.0
3.0
4.0
5.0
6.0
7.0
8.0
9.0
< n >
m = 1.4 a = 1
m = 1.7 a = 0.86
n_b = 3.7

Fig. 3

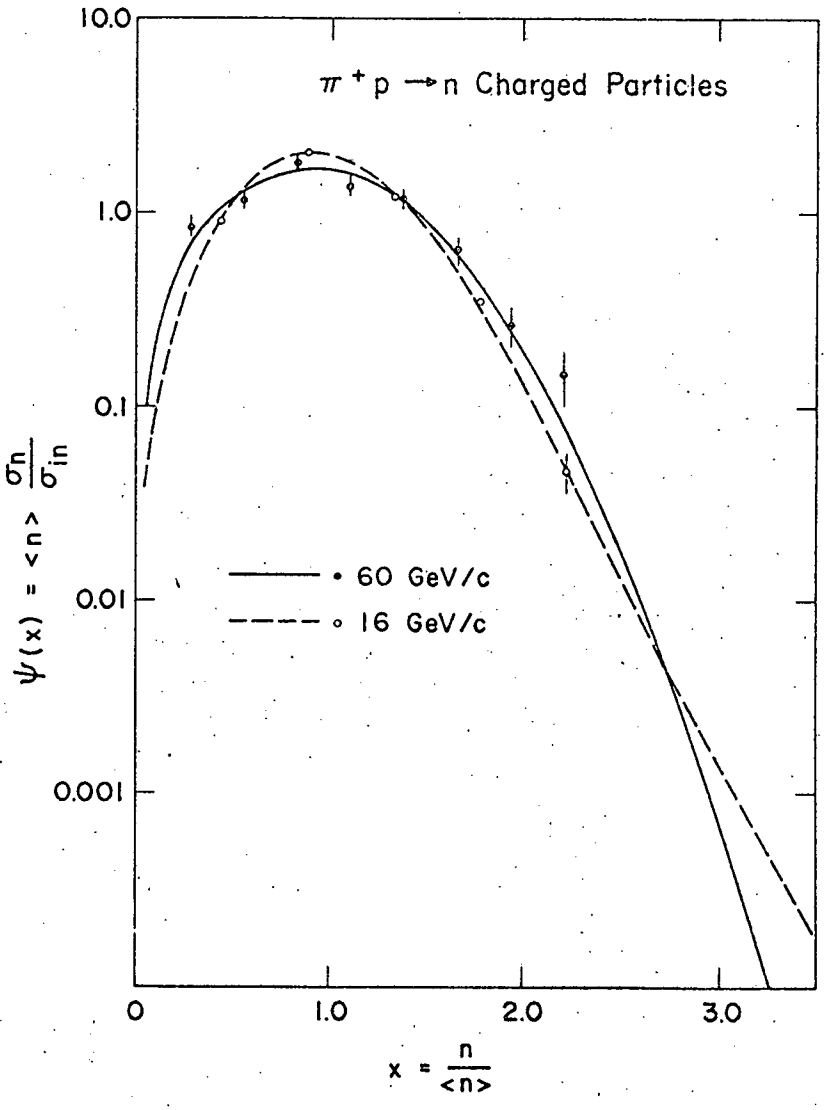
$\pi^+ p \rightarrow n$ Charged Particles
10.0
1.0
0.1
0.01
0.001
$\psi(x) = \langle n \rangle \frac{\sigma_n}{\sigma_{in}}$
• 60 GeV/c
◦ 16 GeV/c
0
1.0
2.0
3.0
$x = \frac{n}{\langle n \rangle}$

Fig. 4

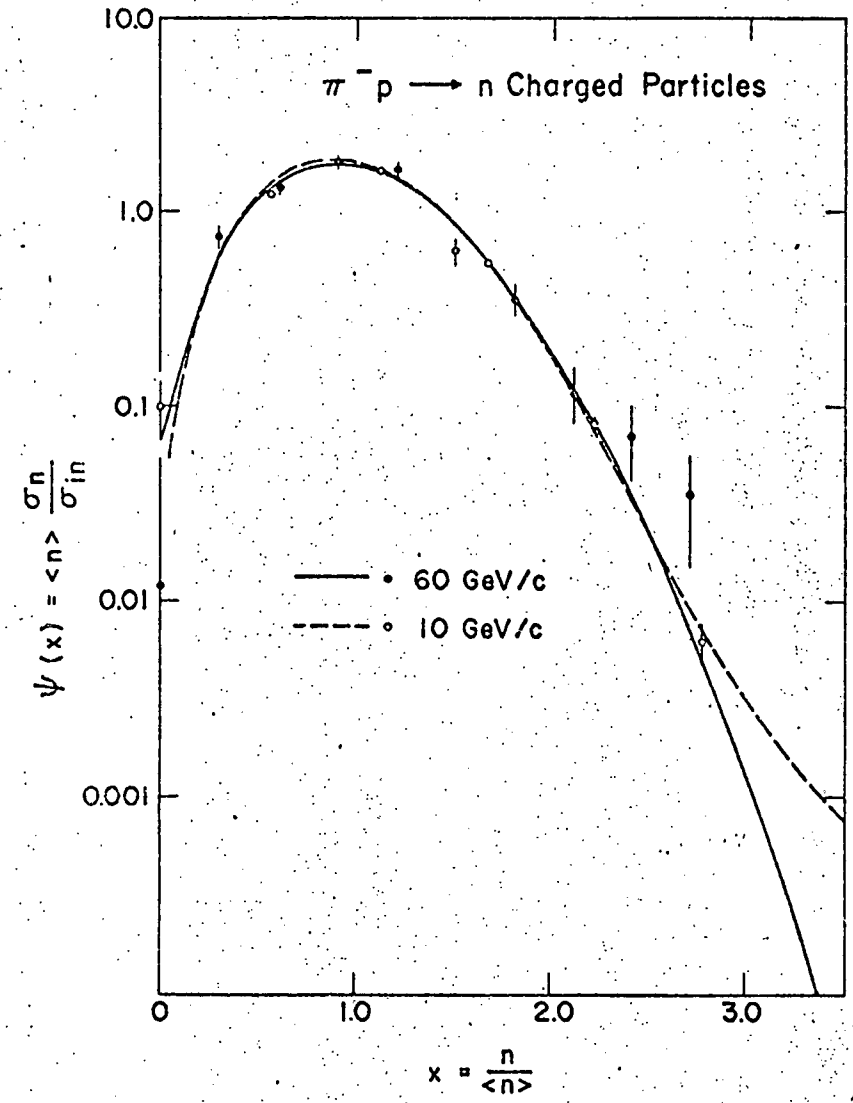
$\pi^- p \longrightarrow$ n Charged Particles
10.0
1.0
0.1
0.01
0.001
$\psi(x) = \langle n \rangle \frac{\sigma_n}{\sigma_{in}}$
• 60 GeV/c
◦ 10 GeV/c
0
1.0
2.0
3.0
$x = \frac{n}{\langle n \rangle}$

Fig. 5

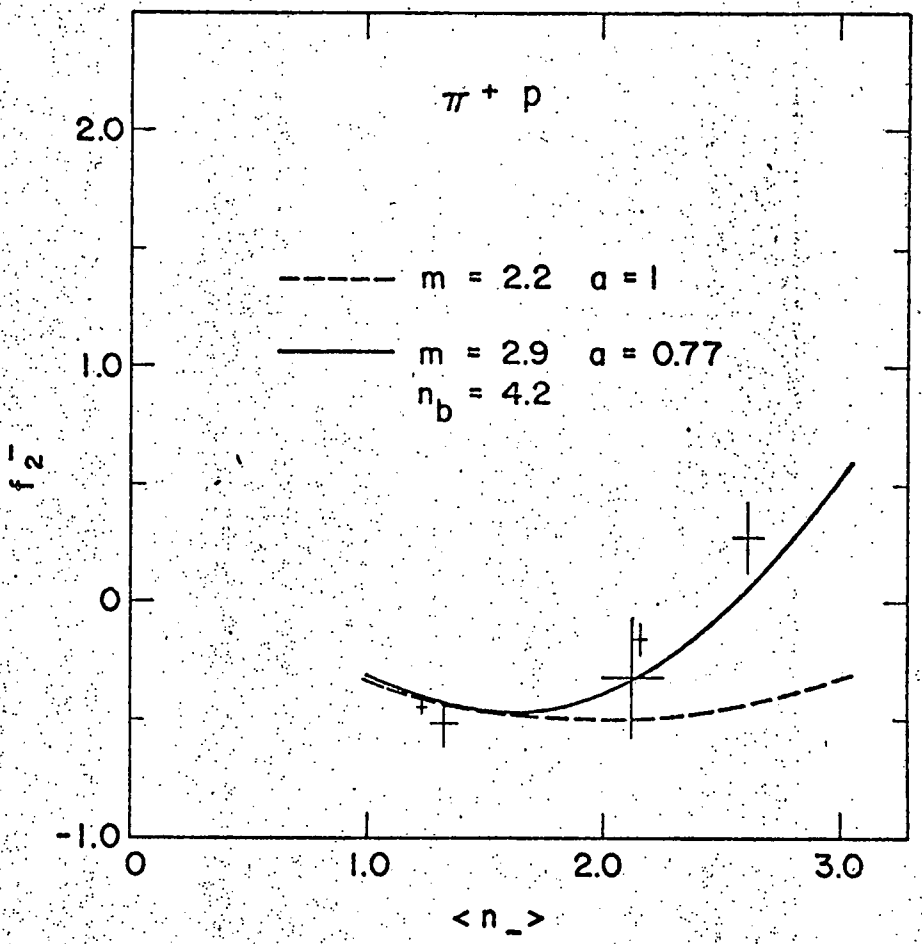
$\pi^+ p$
m = 2.2 a = 1
m = 2.9 a = 0.77
n_b = 4.2
2.0
1.0
0
-1.0
f_2
0
1.0
2.0
3.0
$\langle n_- \rangle$

Fig. 6

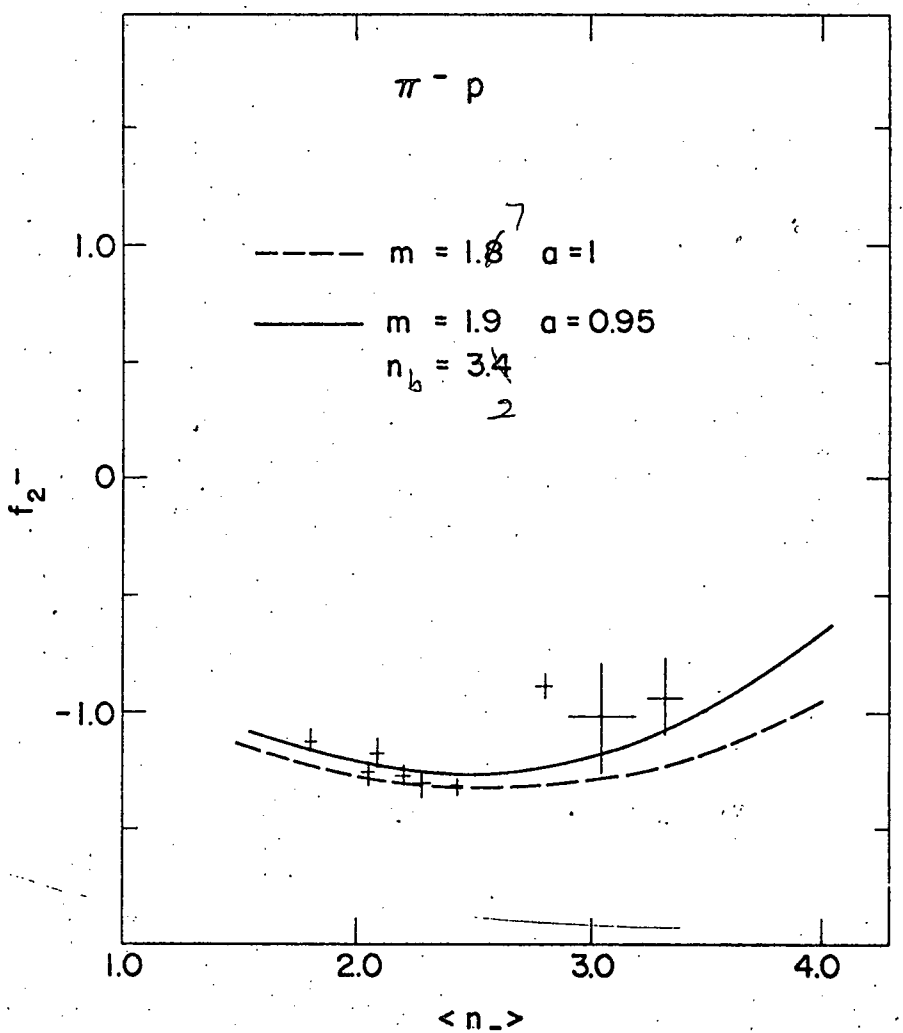
$\pi^- p$
m = 1.87 a = 1
m = 1.9 a = 0.95
n_b = 3.4
2
f_2^-
1.0
0
-1.0
1.0
2.0
3.0
4.0
< n_ >

Fig. 7

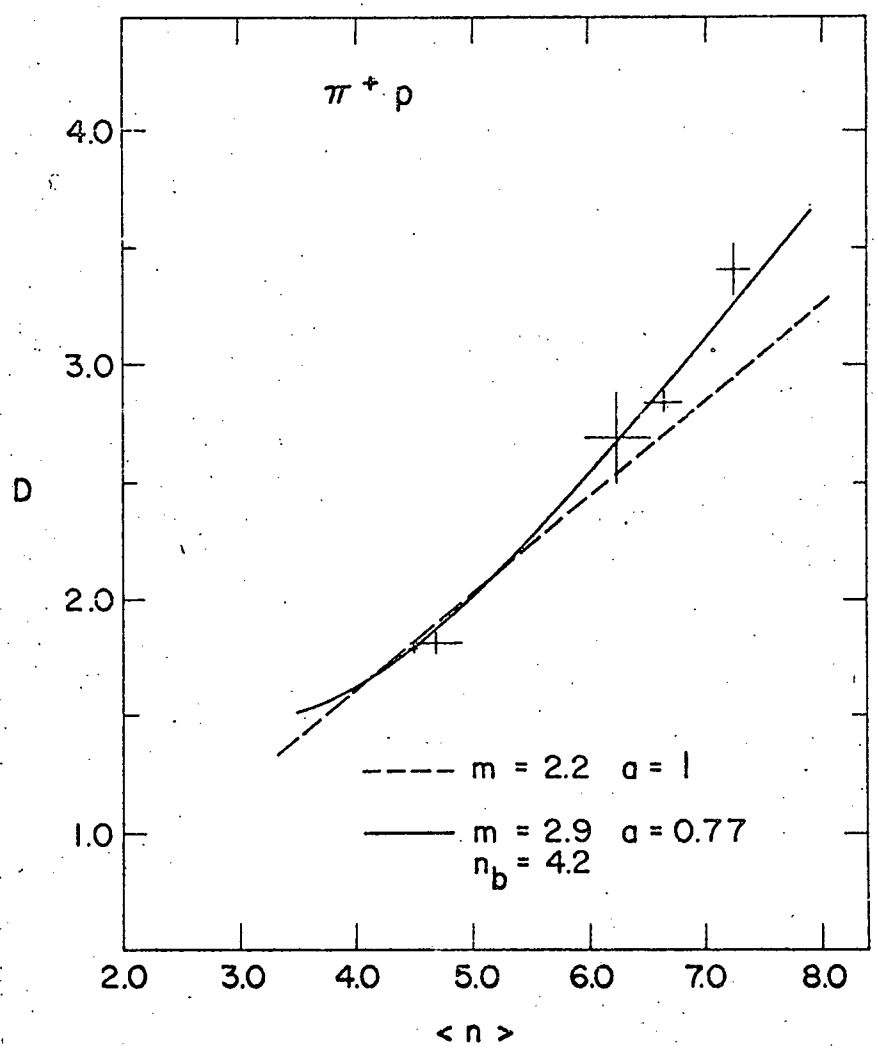
$\pi^+ p$
4.0
3.0
2.0
1.0
D
m = 2.2 a = 1
m = 2.9 a = 0.77
n_b = 4.2
2.0
3.0
4.0
5.0
6.0
7.0
8.0
< n >

Fig. 8

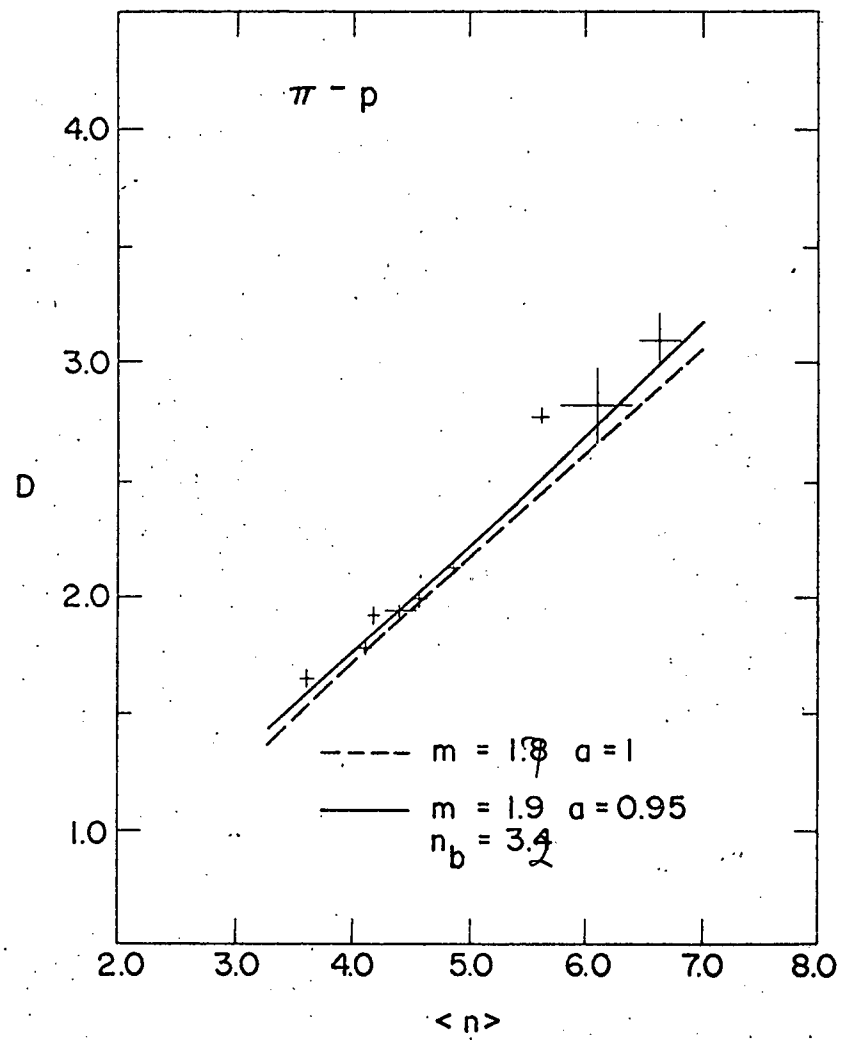
π⁻ p
4.0
3.0
2.0
1.0
D
2.0
3.0
4.0
5.0
6.0
7.0
8.0
< n>
m = 1.8 a = 1
m = 1.9 a = 0.95
n_b = 3.4

Fig. 9

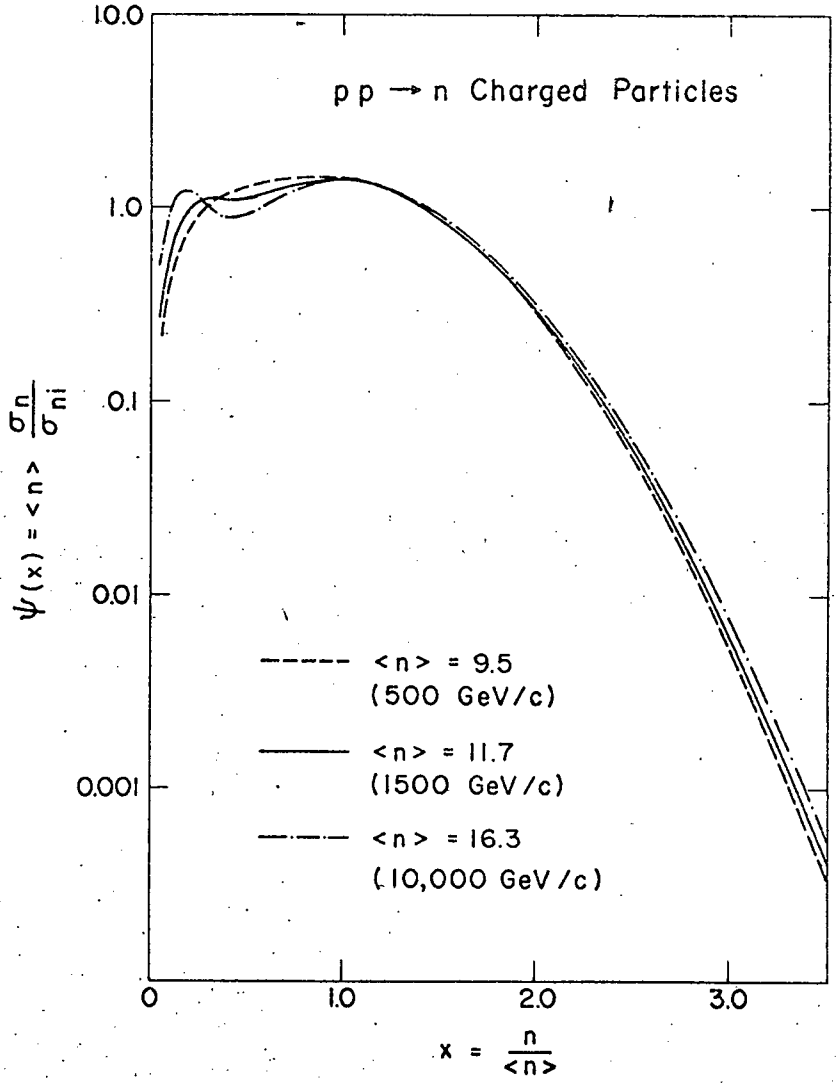
p p → n Charged Particles
10.0
1.0
0.1
0.01
0.001
ψ(x) = < n > σ_n / σ_ni
0
1.0
2.0
3.0
x = n / < n >
< n > = 9.5
(500 GeV/c)
< n > = 11.7
(1500 GeV/c)
< n > = 16.3
(10,000 GeV/c)

Fig. 10

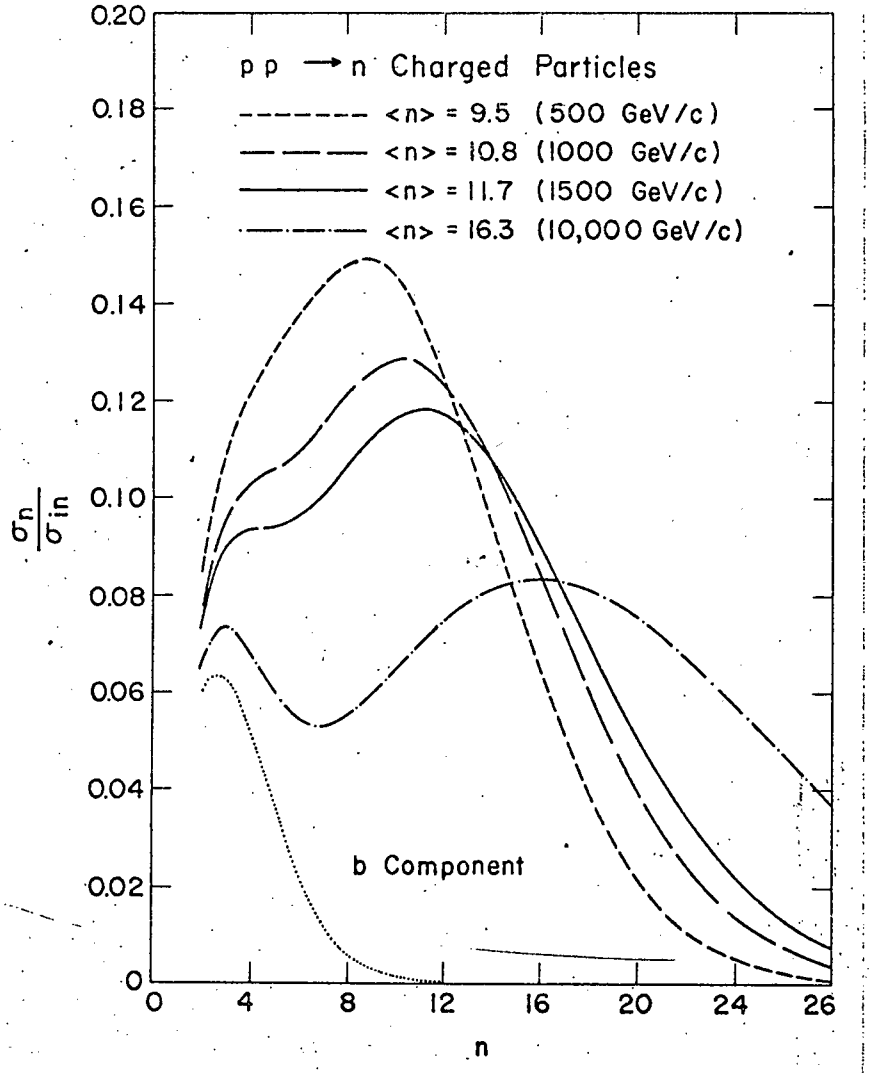
p p → n Charged Particles
<n> = 9.5 (500 GeV/c)
<n> = 10.8 (1000 GeV/c)
<n> = 11.7 (1500 GeV/c)
<n> = 16.3 (10,000 GeV/c)
b Component
$\frac{\sigma_n}{\sigma_{in}}$
n
0.20
0.18
0.16
0.14
0.12
0.10
0.08
0.06
0.04
0.02
0
0
4
8
12
16
20
24
26

Fig. 11

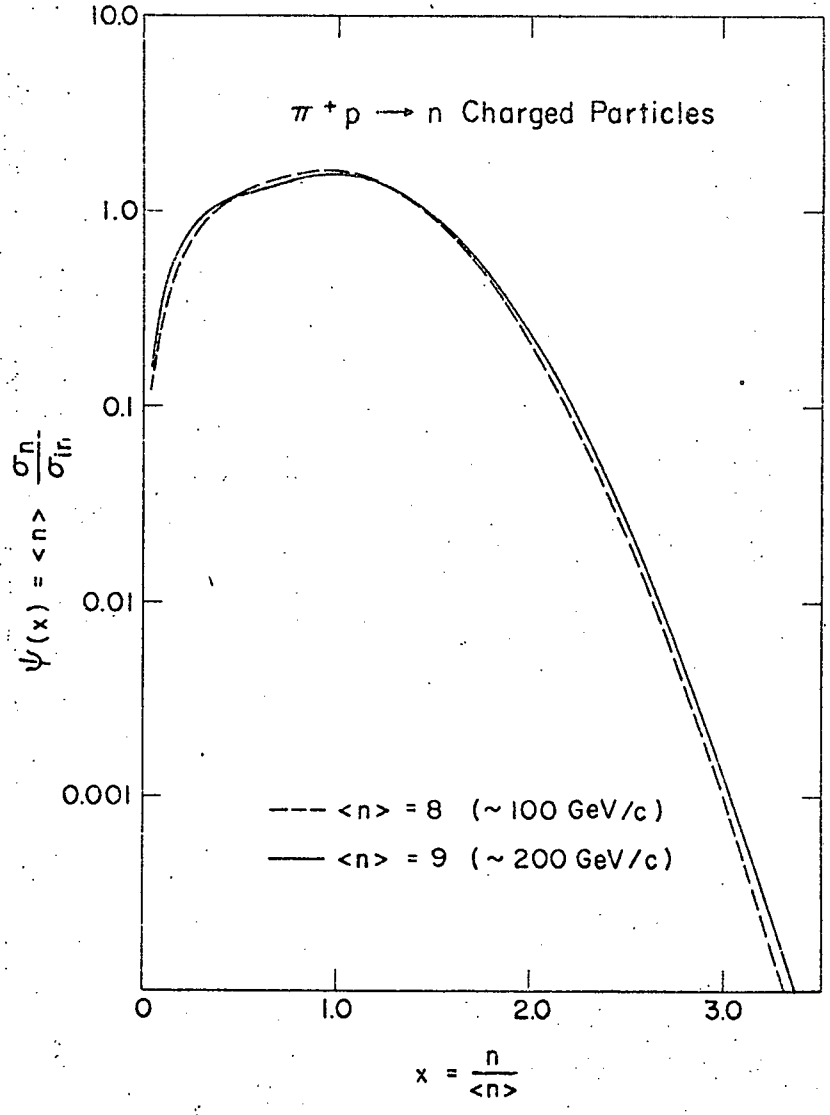
$\pi^+ p \longrightarrow n$ Charged Particles
<n> = 8 (~ 100 GeV/c)
<n> = 9 (~ 200 GeV/c)
$\psi(x) = \langle n \rangle \frac{\sigma_n}{\sigma_{in}}$
$x = \frac{n}{\langle n \rangle}$
10.0
1.0
0.1
0.01
0.001
0
1.0
2.0
3.0

Fig. 12

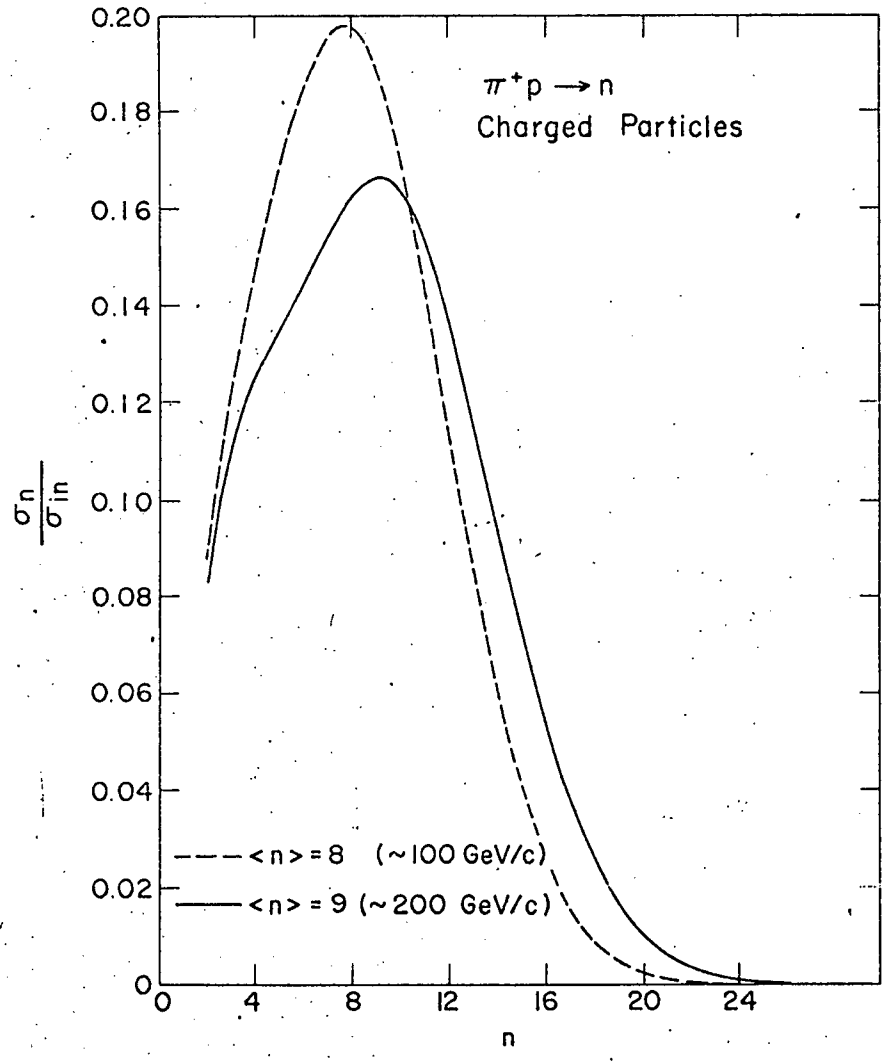
$\pi^+ p \rightarrow n$
Charged Particles
$\frac{\sigma_n}{\sigma_{in}}$
0.20
0.18
0.16
0.14
0.12
0.10
0.08
0.06
0.04
0.02
0
0
4
8
12
16
20
24
n
<n> = 8 (~100 GeV/c)
<n> = 9 (~200 GeV/c)

Fig. 13

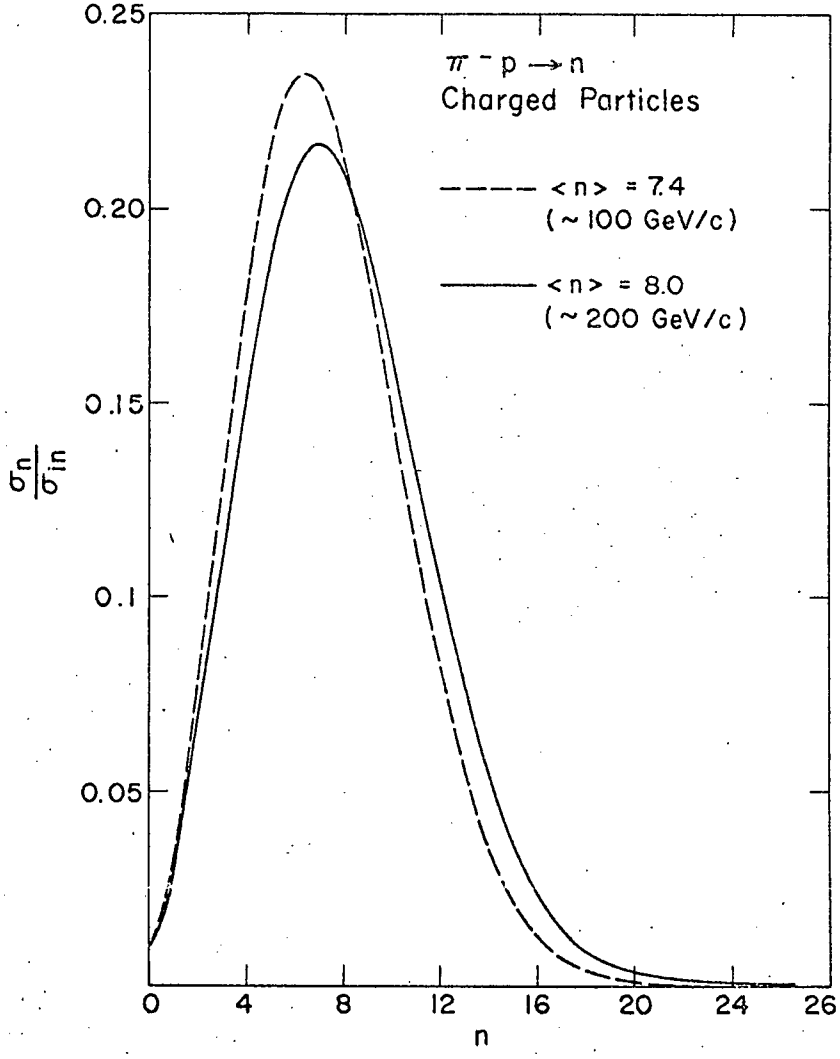
$\pi^- p \rightarrow n$
Charged Particles
$\frac{\sigma_n}{\sigma_{in}}$
0.25
0.20
0.15
0.1
0.05
0
4
8
12
16
20
24
26
n
<n> = 7.4
(~100 GeV/c)
<n> = 8.0
(~200 GeV/c)

Fig. 14